Arch. Metall. Mater. **63** (2018), 3, 1115-1123

DOI: 10.24425/123784

C. HAMILTON*#, S. DYMEK**, A. WĘGLOWSKA***, A. PIETRAS***

NUMERICAL SIMULATIONS FOR BOBBIN TOOL FRICTION STIR WELDING OF ALUMINUM 6082-T6

Aluminum 6082-T6 panels were joined by friction stir welding utilizing a bobbin tool. A thermal simulation of the process was developed based upon machine torque and the temperature dependent yield stress utilizing a slip factor and an assumed coefficient of friction. The torque-based approach was compared to another simulation established on the shear layer methodology (SLM), which does not require the slip factor or coefficient of friction as model inputs. The SLM simulation, however, only models heat generation from the leading edges of the tool. Ultimately, the two approaches yielded matching temperature predictions as both methodologies predicted the same overall total heat generation from the tool. A modified shear layer approach is proposed that adopts the flexibility and convenience of the shear layer method, yet models heat generation from all tool/workpiece interfaces.

Keywords: friction stir welding, bobbin tool, aluminum, simulation, temperature

1. Introduction

Friction stir welding (FSW) and its derivative methods, such as friction stir processing, are now well-established and important technologies in numerous manufacturing sectors, such as the aerospace and automotive industries. Since its introduction by The Welding Institute in 1991, researchers have explored the correlations between the process parameters and the resultant microstructure, mechanical properties, material flow and weld quality during FSW. A tremendous body of knowledge has developed around these issues and has significantly advanced the basic understanding of the interaction between the welding parameters, including shoulder and pin geometries, and the workpieces. Publications by Mishra and Mahoney [1], by Mishra, De and Kumar [2] and by Lowasser and Chen [3] on friction stir welding and processing provide comprehensive literature surveys regarding this extensive body of knowledge. Despite these advances, however, new opportunities in expanding the fundamental knowledge of the FSW process continually present themselves as new tool designs, methods, process improvements, etc. emerge and as investigators apply the FSW process to new materials systems, such as dissimilar metallic materials.

Numerical simulations in conjunction with traditional material characterization techniques, such as optical microscopy, electron microscopy and calorimetry, have proven to be effective tools for analyzing the FSW process. Neto and Neto [4] present an excellent review of the recent achievements in friction stir welding simulation. The foundation for many of these simulations is the transference of machine torque into heat generation within the welding workpieces. For "conventional" welding tools, i.e. tools with a shoulder and pin that act under an applied vertical force and a horizontal force due to the welding velocity, the torque-based simulations have successfully modelled the asymmetric temperature distribution and material flow during the welding process. However, numerous model inputs are required. These include the applied machine forces (vertical and horizontal), the coefficient of friction between the tool and workpieces, μ, and typically, a slip factor that corrects for the efficiency of heat transfer from the tool to the workpieces. Though one may usually know (or measure) the applied forces, selecting an appropriate μ and formulating an apt slip factor can prove problematic.

Colligan and Mishra [5] noted that many FSW simulations assume a coefficient of friction value between 0.3-0.4; however, they also noted that when Kalya et al. [6] correlated the process torque with the welding speed and tool rotation speed for two different aluminum alloys, μ ranged from 0.35 to 1.3. Colligan and Mishra further proposed that μ could be expressed as $3M_e/2F_zR$ where M_e is the measured torque, F_z is the normal (vertical) welding force and R is the shoulder radius. Hamilton et al. [7] in their study of friction stir surfacing (FSS) of aluminum A356 assumed various values for μ in relation to the process pitch, i.e. the distance traveled by the tool per revolution. FSS utilizes a tool without a pin such that the tool shoulder/workpiece interface is the only heat-generating surface. Ignoring plastic deformation in this research, they proposed using a μ value corresponding

* MIAMI UNIVERSITY, DEPARTMENT OF MECHANICAL AND MANUFACTURING ENGINEERING, COLLEGE OF ENGINEERING AND COMPUTING, OXFORD, OHIO, USA
** AGH UNIVERSITY OF SCIENCE AND TECHNOLOGY, FACULTY OF METAL ENGINEERING AND INDUSTRIAL COMPUTER SCIENCE, AL. MICKIEWICZA 30, 30-059 KRAKÓW, POLAND
*** INSTITUTE OF WELDING, DEPARTMENT OF THE TESTING OF MATERIALS WELDABILITY AND WELDED CONSTRUCTION, BŁ. CZESŁAWA STR., 44-100 GLIWICE, POLAND
# Corresponding author: hamiltbc@miamioh.edu

to the static coefficient of friction between A356 and steel (~0.7 as determined by Xie et al. [8]) for small pitch values for which quasi-static conditions hold, but transitioning to the dynamic coefficient of friction (~0.2 as determined by Mandal et al. [9]) for higher pitch values.

Schmidt and Hattel [10], however, considered heat generation from both friction and plastic deformation and proposed the thermal pseudo-mechanical (TPM) model. They demonstrated that for typical FSW conditions, the shear stress at the tool/workpiece interface must be equal to the temperature dependent yield shear stress of the material, τ_{yield}. As such, Schmidt and Hattel expressed the total heat generation, q, as simply $\omega_{tool} r \tau_{yield}$ where ω_{tool} is the angular velocity of the tool and r is the tool radius. The TPM approach, therefore, circumvents the need in simulations to assume a coefficient of friction value and to assign a slip factor, and additionally the TPM approach does not need the welding forces as inputs. Removing the welding forces from a simulation not only "simplifies" the model, but also increases its flexibility as model re-calibration is not necessary when applied to other weld conditions and to other tool geometries, such as the bobbin tool developed by Colligan [11].

The bobbin tool is a variation of the conventional FSW tool that employs two shoulders connected by a pin. With a bobbin tool, rather than the machine applying a vertical force on the tool/workpiece, the workpiece exerts the vertical forces (reactively) on the tool. The welding velocity correlates with the horizontal force on the tool. Threadgill et al. [12] in their study of aluminum 6082-T6 demonstrated that a bobbin tool could produce torque levels equivalent to a conventional tool, but with far less vertical pressure on the tool. From their data, Threadgill measured the bobbin tool torque as 408.6 Nm with a reactive, vertical force of 14.73 kN and the conventional tool torque as 400.2 Nm with an applied, vertical force of 62.38 kN. These values, however, can demonstrate the underlying difficulties of developing a torque-based simulation of the bobbin tool. Consider this: by utilizing the expression for μ presented by Colligan and Mishra [5] and applying it to Threadgill's data [12], the associated μ value for Threadgill's conventional tool would be 0.5, a reasonable value, but the associated μ value for the bobbin tool would be 2.3. Clearly, one needs a modified torque-based approach or an alternate approach to develop a FSW simulation with the bobbin-style tool. To that end, Hilgert et al. [13] successfully developed a shear layer model (SLM) simulation for the friction stir welding of 2024-T3 with a bobbin-style tool based on the TPM approach (a conventional FSW tool was not considered in their work).

In contrast, the work presented here develops a modified torque-based simulation of the bobbin-style tool for the friction stir welding of 6082-T6. Hilgert's SLM approach is also adapted to the 6082-T6 welding, and as will be demonstrated, the two models produce analogous results. The text thoroughly discusses how these simulations generate comparable outcomes, highlighting the similarities and differences between them. Ultimately, a simulation approach that strikes a balance between the advantages of the torque-based and SLM methodologies is developed.

2. Materials and Methods

The Instytut Spawalnictwa (Institute of Welding) in Gliwice, Poland friction stir welded panels of aluminum 6082-T6 alloys in a butt weld configuration utilizing a conventional milling machine specially modified for the process. The workpieces were 250 mm long, 100 mm wide, and 9 mm thick. The Institute employed a bobbin-style tool made of HS6-5-2 high-speed steel with a 28 mm upper shoulder diameter, a 22 mm lower shoulder diameter, a 12 mm pin diameter and a 9 mm pin height. The bobbin tool is schematically rendered in Fig. 1. Each tool shoulder was scrolled with a 2.5 mm pitch, and the pin was threaded from each shoulder with a 3 mm pitch facilitating material flow toward the mid-plane of the workpiece thickness during processing.

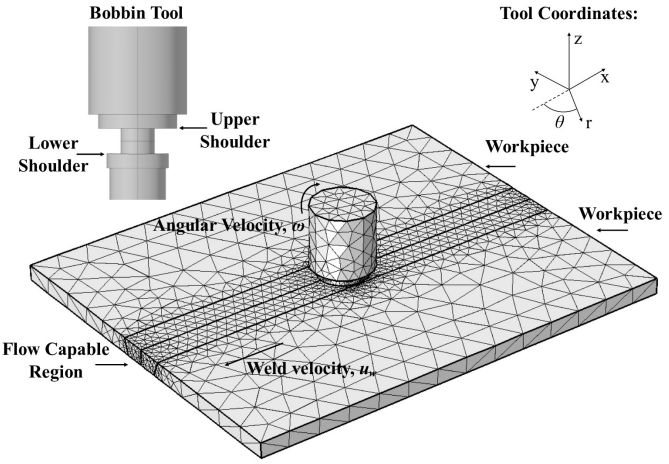

Fig. 1. Computational model of friction stir welding process and schematic of bobbin tool

The Institute performed the welding under two different conditions: 280 RPM tool rotation speed with a weld velocity of 280 mm/min (referred to as the 280/280 condition) and 450 RPM tool rotation speed with a weld velocity of 450 mm/min (referred to as the 450/450 condition). As summarized in Table 1, the transverse welding forces (x-direction) were 2.82 kN and 2.55 kN, respectively, and the measured torques were 143.6 Nm and 121.5 Nm, respectively. St. Węglowski et al. [14] present more details associated with the capabilities of the FSW equipment, such as the force and torque measurements. To verify the welding simulations, the temperature profile across the weld zone was captured using a Vigocam v50 Thermal Imaging Camera (temperature range: 263 K-773 K (–10°C-500°C); ±2%

TABLE 1

Summary of friction stir weld conditions and parameters

Tool Rotation Speed (RPM)	Tool Angular Velocity, ω (s^{-1})	Weld Velocity, u_w (mm/min)	Transverse Force, F_x (kN)	Torque, M (Nm)
280	29.3	280	2.82	143.6
450	47.1	450	2.55	121.5

accuracy). All temperature measurements were performed in air atmosphere at a temperature of 20°C and a relative humidity of 50% in daylight. The thermal emissivity for the infrared data was calibrated and determined to be 0.4.

3. Results and Discussion

3.1. Modified Torque-Based Approach

Fig. 1 displays the friction stir welding process as modeled in the modified torque-based simulation along with a schematic of the bobbin tool profile. The basis for the simulation is the numerical model for temperature distribution and material flow developed by Hamilton et al. [15] for a conventional FSW tool. The bobbin-tool model contains 25506 tetrahedral elements, 7126 triangular elements, 936 edge and 68 vertex elements. The temperature dependent thermal conductivity, k, and the specific heat capacity, c_p, of aluminum 6082-T6 are taken from Gao et al. [16] and from Zahra et al. [17], respectively. In addition to appropriate boundary conditions, Hamilton et al. also detail the viscosity calculations, and to that end, Table 2 presents the Q, A, α and n values (taken from Wang et al. [18]) utilized to calculate the flow stress for 6082-T6 based on the Sheppard-Wright formulation.

TABLE 2

Material constants for the Sheppard and Wright flow stress equation and Zener-Hollomon parameter

Material Constant	Value	Units
Q	168000	J mol^{-1}
A	3.0197×10^{11}	s^{-1}
α	0.02416	MPa^{-1}
n	4.70929	n/a

For a conventional tool and perfect sliding conditions, i.e. heat generation due only to friction, the following equation describes the heat flux at the tool/workpiece interfaces:

$$q = \delta \mu P_N \left(\omega r - u_w \sin\theta \right) \tag{1}$$

where δ is a slip factor, μ is the coefficient of friction between the tool and the workpiece, P_N is the normal pressure relative to the interface, r is the radial distance measured from the tool center, θ is the radial angle measured about the tool axis, and u_w is the weld velocity. Hamilton et al. [19] expressed the slip factor in terms of the welding temperature, T, relative to the solidus temperature, T_s, of the workpiece alloy, $\delta = e^{-(4T/7Ts)}$, and this definition is adopted in the torque-based simulation. The value for the coefficient of friction was set to 0.6 based on the guidelines set forth by Hamilton et al. [7].

For a conventional tool, machine settings determine P_N for the shoulder/workpiece interface, which, therefore, serves as an input for the model. For the bobbin tool, however, the forces acting on the tool shoulders (upper and lower) derive from the reaction of the workpiece, rather than from a force exerted by the FSW machine. To that end, the model presented here initially assumes that the separation between the bobbin tool shoulders, i.e. the pin length, is exactly equivalent to the workpiece thickness. At room temperature and at time equal to zero, the model adopts zero as the magnitude of the forces on the tool shoulders. As welding begins, therefore, the pin/workpiece interface is initially the only interaction responsible for heat generation, but as the welding temperature increases, the workpiece thickness will thermally expand and exert a normal pressure (in the z-direction), $(P_N)_{\exp}$, on the bobbin tool shoulders as given by:

$$\left(P_N \right)_{\exp} = \alpha E \left(T - T_{rm} \right) \tag{2}$$

where α is the coefficient of thermal expansion, E is the elastic modulus, T is the welding temperature and T_{rm} is room temperature. All tool/workpiece interfaces now contribute to heat generation as welding progresses.

The pressure exerted by the workpiece on the tool shoulders will increase with increasing weld temperature until the pressure reaches the temperature dependent yield strength of the material, $\sigma_y(T)$. Beyond this point, the pressure becomes equivalent to the yield strength value. The simulation, therefore, assigns the value for the normal pressure on the tool shoulders as the minimum between $(P_N)_{\exp}$ and $\sigma_y(T)$. Temperature dependence of the yield stress, $\sigma_y(T)$, is captured in the following equation presented by Tutum and Hattel [20]:

$$\sigma_y \left(T \right) = \sigma_{y,ref} \left(1 - \frac{\left(T - T_{ref} \right)}{\left(T_s - T_{ref} \right)} \right) \tag{3}$$

where $\sigma_{y,ref}$ is the room temperature yield stress of the workpiece (276 MPa), T_s is the solidus temperature of the workpiece (855 K) and T_{ref} is room temperature (293 K). With this modification, the simulation utilizes Eq. (1) for heat generation. Inputs for the model then become the normal pressure on the pin (as determined by the weld velocity in the x-direction and typically measured) and the coefficient of friction.

For a conventional tool, Hamilton et al. [7] assigned the maximum strain rate associated with the tool shoulder to the entire flow capable region. However, since the bobbin tool has two shoulders, the simulation must also modify the manner in which the strain rate of the flow capable region is treated. Consequently, the model assumes that the strain rate of the flow capable region decreases linearly from the upper tool shoulder, $\dot{\varepsilon}_{us}$, to a minimum strain rate at the mid-plane thickness of the workpiece, $\dot{\varepsilon}_{pin}$, and then increases again linearly to the lower tool shoulder, $\dot{\varepsilon}_{ls}$. These values are given by:

$$\dot{\varepsilon}_{us} = \frac{r_{us}\omega}{\frac{h}{2}\sqrt{3}}, \quad \dot{\varepsilon}_{pin} = \frac{r_{pin}\omega}{\frac{h}{2}\sqrt{3}}, \quad \dot{\varepsilon}_{ls} = \frac{r_{ls}\omega}{\frac{h}{2}\sqrt{3}} \tag{4}$$

where r_{us} is the upper shoulder radius, r_{ls} is the lower shoulder radius, r_{pin} is the pin radius at the mid-plane thickness, ω is the angular velocity of the tool and h is the workpiece thickness. Otherwise, the modified torque-based approach retains the slip

factor derived from the welding temperature/solidus temperature ratio, and viscosity calculations and boundary conditions for material flow as are those described by Hamilton et al. [7] and Hamilton et al. [19].

3.2. Verification

As previously noted, weld temperatures were experimentally recorded by a thermal imaging camera for the two weld conditions. Specifically, the thermal camera recorded the maximum weld temperature on the surface of the workpieces at a location just behind the tool (~0.5 mm). Table 3 summarizes these measured weld temperatures along with the weld temperatures predicted by the modified torque-based model at this same location. As seen in the table, for the 280/280 condition, the measured welding temperature is 702 K ±14.0 K (429°C ±8.6°C) compared with 713K (440°C) predicted by the simulation. For the 450/450 condition, the measured temperature is 732 K ±14.6 K (459°C ±9.2°C) compared with 723 K (450°C) predicted by the simulation. Table 4 summarizes the measured torque values for the two welding conditions and those torque values predicted by the simulation. As seen in the table, for the 280/280 condition the measured torque is 143.6 Nm while that predicted by the simulation is 184.0 Nm. For the 450/450 condition the measured torque is 121.5 Nm, and the predicted torque is 159.0 Nm. Though the model does over predict the welding torque, the good agreement between the measured and predicted temperatures validates the modified torque-based model approach for the friction stir welding of 6082-T6 with a bobbin style tool.

TABLE 3

Comparison of measured welding temperatures to predicted temperatures

FSW Condition	Experimental Temperature	Modified Torque-Based Model	Shear Layer Model
280/280	702 K ±14.0 K (429°C ±8.6°C)	713 K (440°C)	682 K (409°C)
450/450	732 K ±14.6 K (459°C ±9.2°C)	723 K (450°C)	685 K (412°C)

TABLE 4

Comparison of measured torque values to predicted torque values

FSW Condition	Measured Torque (Nm)	Modified Torque-Based Model (Nm)	Shear Layer Model (Nm)
280/280	143.6	184.0	169.7
450/450	121.5	159.0	145.9

3.3. Shear Layer Model Approach

The shear layer model (SLM) developed by Hilgert et al. [13] for the friction stir welding of 2024-T3 using a bobbin tool was adapted for the friction stir welding of 6082-T6. As previously discussed, a primary difference between the two approaches is that under the SLM methodology, the heat generation at the tool/workpiece interface is given by:

$$q = \omega r \tau(T) \tag{5}$$

where ω is the angular velocity of the tool, r is the radial distance measured from the tool center and $\tau(T)$ is the temperature dependent yield shear stress of the material. Unlike the heat generation formulation in Eq. (1), the formulation in Eq. (5) does not include the coefficient of friction or a slip factor. For the simulation of 2024-T3, Hilgert utilized experimental yield shear stress versus temperature data taken from the Metals Handbook of The American Society for Metals [20]. For the adaptation of the SLM approach to the joining of 6082-T6, the temperature dependent yield shear stress is captured by simply dividing the $\sigma_y(T)$ expression in Eq. (3) by $\sqrt{3}$ in accordance with the Von Mises relationship between the yield stress and the yield shear stress. Hilgert did not provide details concerning tool tilt angle, strain rate and/or viscosity calculations in the SLM approach, so the adaptation of SLM to 6082-T6 handles these parameters/calculations in exactly the same methodology as the modified torque-based approach.

Another major difference between the SLM and modified torque-based approaches is which tool/workpiece interfaces contribute to heat generation. In the modified torque-based approach outlined in the previous section, *all* tool/workpiece interfaces

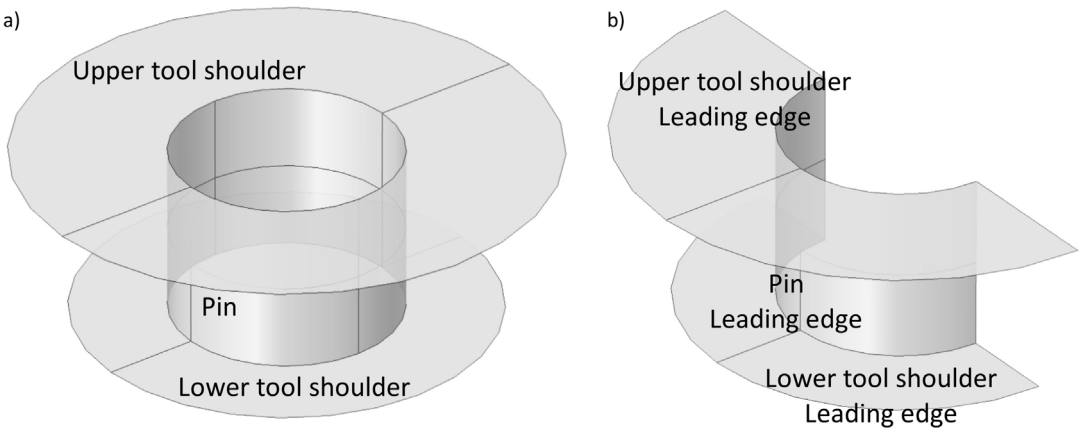

Fig. 2. Heat generating interfaces in the simulations: a) modified torque-based approach, b) SLM approach

contribute to heat generation. In the SLM approach developed by Hilgert, however, only the *leading edge* tool/workpiece interfaces contribute to heat generation, as schematically shown in Fig. 2. Therefore, in the adaptation of SLM to 6082-T6, only the front halves of the upper shoulder, lower shoulder and pin interfaces with the workpiece contribute to heat generation. Under these constraints, Table 3 presents the predicted weld temperatures from the SLM approach taken at the same location as the measured temperatures and the modified torque-based approach. As seen in the table, the SLM approach under predicts the welding temperature for both weld conditions; however, the difference is only 5% for the 280/280 condition and 10% for the 450/450 condition. The SLM approach also shows good agreement with the modified torque-based approach with less than 10% difference in the temperature predictions between the two approaches for both weld conditions. Table 4 presents the predicted torque values from the SLM approach. Like the modified torque-based approach, the SLM approach also over predicts the torque during welding, though closer to the measured values. The difference between the torque values predicted from the two approaches, however, is again less than 10% for both weld conditions.

Fig. 3 shows the predicted temperature profiles taken across the weld zone at the mid-plane thickness just behind the pin. The figure demonstrates the excellent agreement in the temperature distribution from the two approaches even up to 50 mm from either side of the weld centerline. The most notice-

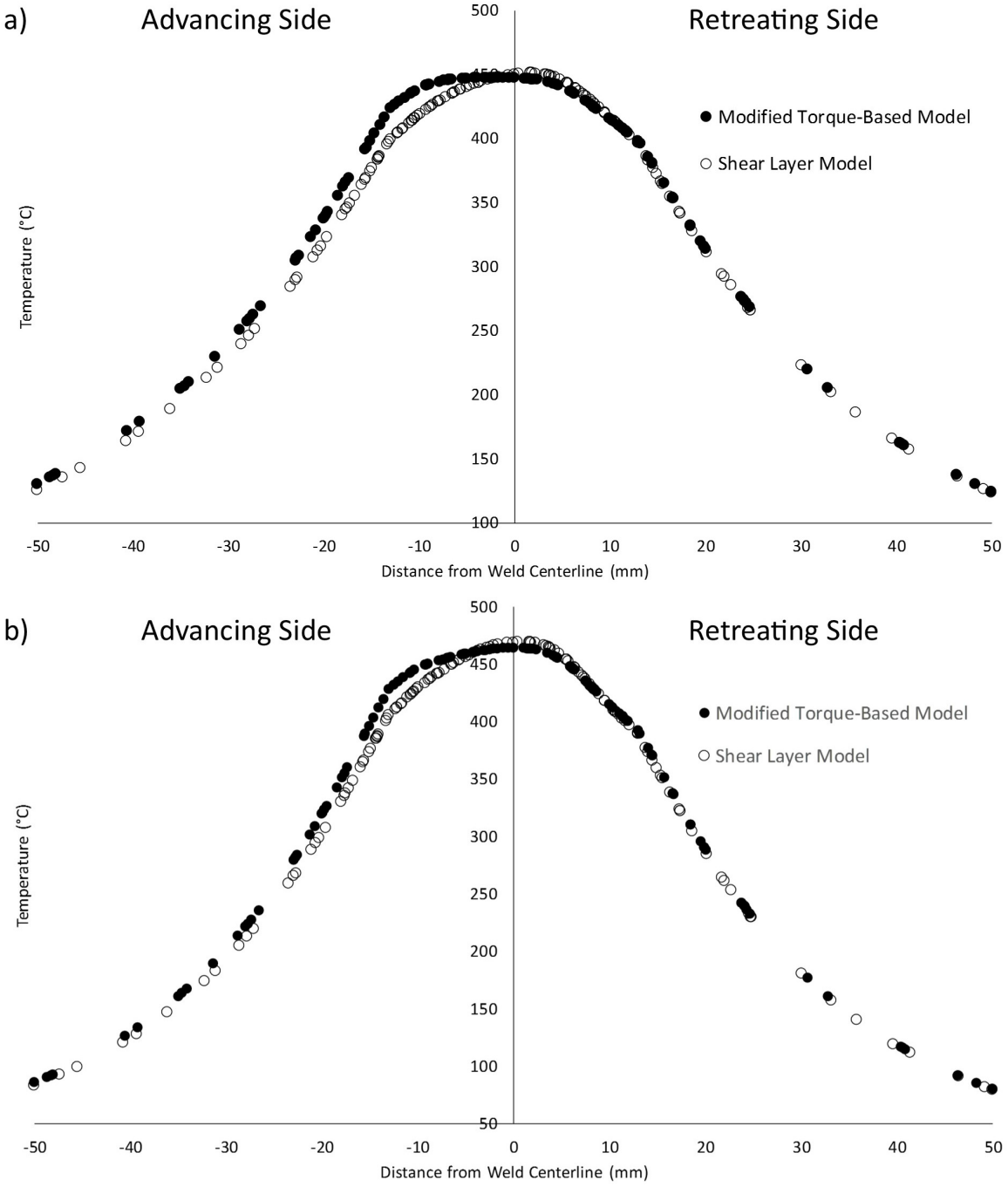

Fig. 3. Mid-plane temperature profiles from the torque-based and SLM simulations: a) 280/280 condition and b) 450/450 condition

able temperature discrepancy between the two models occurs on the advancing side, approximately 12-15 mm from the weld centerline. For both weld conditions, the torque-based approach predicts a higher temperature (~6%) than the SLM in this area of the weld. Overall, however, the two models yield very similar temperature profiles across this weld zone region.

3.4. Comparison of the Torque-based Approach and SLM Approach

A reasonable question to ask is how these disparate simulation approaches can produce, at least in the case of a bobbin tool, such similar results, particularly in the temperature distributions at the mid-plane thickness. One approach leans upon an assumed value for the coefficient of friction and a temperature-based slip factor, while the other assumes that the temperature dependent yield shear stress dominates at the tool/workpiece interfaces. To address this question, begin by considering the heat flux expression for the two models, Eq. (1) (torque-based) and Eq. (5) (SLM). The heat flux equation for the modified torque-based approach can be simplified by recognizing that for typical FSW rotation speeds and welding velocities, the $u_x \sin\theta$ term in Eq. (1) becomes small relative to the ωr term. As such, the $(\omega r - u_x \sin\theta)$ term may be effectively replaced by ωr, and Eq. (1) simplifies to:

$$q = \delta \mu P_N \omega r \tag{6}$$

where all terms have their previous meaning. As previously discussed, the P_N term from the torque-based approach is the pressure normal to the tool/workpiece interface. For the bobbin-style tool, the thermal expansion of the material generates this pressure on the tool shoulders and reaches a maximum value equivalent to the temperature dependent yield stress of the material, $\sigma_y(T)$ from Eq. (3). The pin pressure, $(P_N)_{pin}$, under the torque-based approach is derived from the measured horizontal force during processing.

Eqs. (5) and (6) represent the heat fluxes at the tool/workpiece interfaces. There are two major differences between the modified torque-based approach and the SLM approach: 1) the torque-based approach assumes that all tool/workpiece interfaces contribute to heat generation while the SLM approach assumes that only the leading edge interfaces contribute to heat generation and 2) the torque-based approach uses a measured horizontal force to determine the pressure on the pin while the SLM approach uses the temperature dependent yield shear stress as the pin pressure. The heat generated at any tool/workpiece interface, Q, may be written as:

$$Q = \int_{\theta_1}^{\theta_2} \int_{r_1}^{r_2} q r dr d\theta \tag{7}$$

where θ and r are the polar coordinates associated with the interface. Total heat generation would then be the sum of the individual contributions from the upper shoulder, the lower shoulder and the pin. Therefore, the ratio of total heat generation from the SLM approach to the total heat generation from the torque-based approach, R_Q, may be expressed as:

$$R_Q = \frac{\begin{array}{l} \int_{-\frac{\pi}{2}}^{\frac{\pi}{2}} \int_{r_{pin}}^{r_{us}} \omega r \tau(T) r dr d\theta + \\ + \int_{-\frac{\pi}{2}}^{\frac{\pi}{2}} \int_{r_{pin}}^{r_{ls}} \omega r \tau(T) r dr d\theta + \\ + \int_{-\frac{\pi}{2}}^{\frac{\pi}{2}} \omega r_{pin} \tau(T) h r_{pin} d\theta \end{array}}{\begin{array}{l} \int_0^{2\pi} \int_{r_{pin}}^{r_{us}} \delta \mu \omega r \sigma_y(T) r dr d\theta + \\ + \int_0^{2\pi} \int_{r_{pin}}^{r_{ls}} \delta \mu \omega r \sigma_y(T) r dr d\theta + \\ + \int_0^{2\pi} \delta \mu \omega r_{pin} (P_N)_{pin} h r_{pin} d\theta \end{array}} \tag{8}$$

where all terms have their previous meaning. The angular integrations from $-\pi/2$ to $\pi/2$ in the numerator indicate heat generation occurring only at the leading edges of tool/workpiece interfaces under the SLM approach, whereas under the torque-based approach heat generation occurs at the leading and trailing edges of the tool, and the corresponding integrations are from 0 to 2π. Evaluating the integrals and eliminating common terms yields:

$$R_Q = \frac{\begin{array}{l} \frac{1}{3}\tau(T)\left(r_{us}^{\,3} - r_{pin}^{\,3}\right) + \\ + \frac{1}{3}\tau(T)\left(r_{ls}^{\,3} - r_{pin}^{\,3}\right) + \tau(T) h r_{pin}^{\,2} \end{array}}{2\delta\mu \left[\begin{array}{l} \frac{1}{3}\sigma_y(T)\left(r_{us}^{\,3} - r_{pin}^{\,3}\right) + \\ + \frac{1}{3}\sigma_y(T)\left(r_{ls}^{\,3} - r_{pin}^{\,3}\right) + \\ + (P_N)_{pin} h r_{pin}^{\,2} \end{array}\right]} \tag{9}$$

But by Von Mises, the temperature dependent yield shear yield stress, $\tau(T)$, is related to $\sigma_y(T)$ in the following manner:

$$\tau(T) = \frac{\sigma_y(T)}{\sqrt{3}} \tag{10}$$

Therefore, the heat ratio may be further simplified to the following:

$$R_Q = \frac{\frac{1}{3}\left(r_{us}^{\,3} - r_{pin}^{\,3}\right) + \frac{1}{3}\left(r_{ls}^{\,3} - r_{pin}^{\,3}\right) + h r_{pin}^{\,2}}{2\delta\mu\sqrt{3}\left[\begin{array}{l} \frac{1}{3}\left(r_{us}^{\,3} - r_{pin}^{\,3}\right) + \frac{1}{3}\left(r_{ls}^{\,3} - r_{pin}^{\,3}\right) + \\ + \frac{(P_N)_{pin}}{\sigma_y(T)} h r_{pin}^{\,2} \end{array}\right]} \tag{11}$$

From the torque-based simulations for the two weld conditions, the average value of the $(P_N)_{pin}/\sigma_y(T)$ ratio across all pin/workpiece interfaces is ~0.30, and the average value of the slip factor, δ, across all tool/workpiece interfaces is ~0.60. The selected value for the coefficient of friction, μ, is 0.60 in accord-

ance with Hamilton et al. [7]. Substituting these values and the actual tool dimensions into Eq. (11) yields:

$$R_Q = \frac{\frac{1}{3}\left(14^3 - 6^3\right) + \frac{1}{3}\left(11^3 - 6^3\right) + (9)(6)^2}{2(0.60)(0.60)\sqrt{3}\left[\begin{array}{l}\frac{1}{3}\left(14^3 - 6^3\right) + \\ +\frac{1}{3}\left(11^3 - 6^3\right) + \\ +(0.30)(9)(6)^2\end{array}\right]} = 0.94 \quad (12)$$

Despite the dissimilarities between the modified torque-based approach and the SLM approach, the difference between total heat generations from the two models is less than 6% for the welding conditions studied. Therefore, the excellent agreement between the temperature distributions from the two approaches is not surprising. The torque-based approach predicts slightly more heat generation than the SLM approach, which then accounts for the slightly higher (~6%) temperature predictions by the torque-based approach on the advancing side of the weld.

Closer examination reveals that the torque-based approach effectively models greater heat generation at the tool shoulders than the SLM approach, but that, conversely, the SLM approach models more heat generation at the pin than the torque-based approach. Under the torque-based approach, the shoulders account for 89% of the total heat generation, and the pin accounts for 11%. Under the SLM approach, the shoulders account for only 81% of the total heat generation, and the pin, therefore, accounts for 19%. The net effect is that both approaches predict essentially the same total heat generation from the tool. It should be noted again, however, that the SLM approach assumes that only the leading edges of the tool contribute to heat generation. If the SLM approach used both the leading and trailing edges of the tool for heat generation as the torque-based approach does, the total heat generation of the SLM model would be substantially higher than that of the torque-based model. In fact, the R_Q ratio would double from 0.94 to 1.88.

3.5. Modified Shear Layer Model Approach

The convenience of the SLM approach, i.e. no input parameters other than the yield shear stress of the material, tool dimensions and rotation speed, is extremely attractive; however, assuming that heat generation occurs at both the leading and trailing edges of the tool, as prescribed in the modified torque-based approach, also stands to reason. Perhaps, therefore, a middle ground can be found between the two approaches. The foundation of the SLM approach is the thermal pseudo-mechanical (TPM) formulation from Schmidt and Hattel [10]. The TPM method states that the total heat flux at the tool/workpiece interface from both plastic deformation and Coulomb friction is given by:

$$q_{total} = \omega_{tool} r\left(\lambda \tau_{yield} + (1-\lambda)\tau_{friction}\right) \quad (13)$$

where $\tau_{friction}$ is the frictional shear stress acting on the interface, λ is a contact state variable defined as the ratio of the angular velocity of the matrix to the angular velocity of the tool and all other terms have their previous meaning. The state variable essentially partitions the heat generation between plastic deformation and friction such that when perfect sticking dominates $\lambda = 1$ and when perfect sliding dominates $\lambda = 0$. Schmidt and Hattel noted that even if a small amount of sticking occurs, the frictional shear stress must be equal to the yield shear stress of the material. As such, Eq. (13) reduces to the expression presented in Eq. (5).

Eq. (13), however, assumes perfect heat transfer to the workpiece, i.e. 100% efficiency, under either plastic or frictional heat generation conditions. In contrast, the slip factor, δ, in Eq. (1) is specifically introduced to account for inefficiencies in heat transfer that can arise as the tool/workpiece interface softens as the welding temperatures approach the solidus temperature of the workpiece(s). Similarly, Nandan et al. [22] utilized a mechanical efficiency factor, η, associated with the heat generation from plastic deformation. Introducing these concepts into Eq. (13), the total heat flux can be rewritten as:

$$q_{total} = \omega r\left(\eta_p \lambda \tau_{yield} + \eta_f (1-\lambda)\tau_{friction}\right) \quad (14)$$

Where η_p and η_f are the heat transfer efficiencies associated with plastic deformation and friction, respectively. The state variable, λ, is typically very small. For example, Heurtier et al. [23] estimated the value to be 1/100 based on microstructural observations in 2024-T3. As such, heat generation by friction dominates, but as noted by Schmidt and Hattel even for small values of λ, the frictional shear stress will equal the yield shear stress. Therefore, introducing the temperature dependent yield shear stress, $\tau(T)$, as the frictional stress and eliminating the plastic deformation component due to the small value of λ, Eq. (13) becomes:

$$q_{total} = \eta_f \omega r \tau(T) \quad (15)$$

which is equivalent to Eq. (5) with the exception of the frictional efficiency factor, η_f. Conceivably, therefore, Eq. (15) forms the basis of a modified-SLM approach.

To find an approximate value for η_f, begin by imposing two criteria: 1) that the modified-SLM approach assume heat generation occurs at all tool/workpiece interfaces and 2) that the modified-SLM approach and torque-based approach yield the same amount of total heat generation. Under these conditions, Eq. (8) can be rewritten as:

$$\frac{\begin{array}{l}\int_0^{2\pi}\int_{r_{pin}}^{r_{us}} \eta_f \omega r \tau(T) r dr d\theta + \\ +\int_0^{2\pi}\int_{r_{pin}}^{r_{ls}} \eta_f \omega r \tau(T) r dr d\theta + \\ +\int_0^{2\pi} \eta_f \omega r_{pin} \tau(T) h r_{pin} d\theta\end{array}}{\begin{array}{l}\int_0^{2\pi}\int_{r_{pin}}^{r_{us}} \delta \mu \omega r \sigma_y(T) r dr d\theta + \\ +\int_0^{2\pi}\int_{r_{pin}}^{r_{ls}} \delta \mu \omega r \sigma_y(T) r dr d\theta + \\ +\int_0^{2\pi} \delta \mu \omega r_{pin} (P_N)_{pin} h r_{pin} d\theta\end{array}} = 1 \quad (16)$$

where the limits of integration in the numerator are now 0 to 2π, indicating that heat generation at both the leading *and* trailing edges is taken into account. Solving for η_f yields a value of 0.53. For convenience, let the general value of η_f be 0.5, which is the same value that Nandan et al. [22] used as the mechanical efficiency associated with heat transfer from plastic deformation.

Modified-SLM simulations were then created based upon the heat flux expression in Eq. (15). In these simulations, the leading and trailing edges of the tool, both shoulder and pin, were modeled as heat generating interfaces. All other aspects of the simulations, i.e. strain rate calculations, viscosity calculations, boundary conditions, etc., were the same as the torque-based and SLM simulations previously discussed. Table 5 presents the predicted temperatures from the new simulations in relation to the measured weld temperatures and reveals the excellent agreement between them. Fig. 4 displays the temperature distribution

TABLE 5

Comparison of measured welding temperatures to modified-SLM predicted temperatures

FSW Condition	Experimental Temperature	Modified-SLM
280/280	702 K ±14.0 K (429°C ±8.6°C)	702 K (429°C)
450/450	732 K ±14.6 K (459°C ±9.2°C)	717 K (444°C)

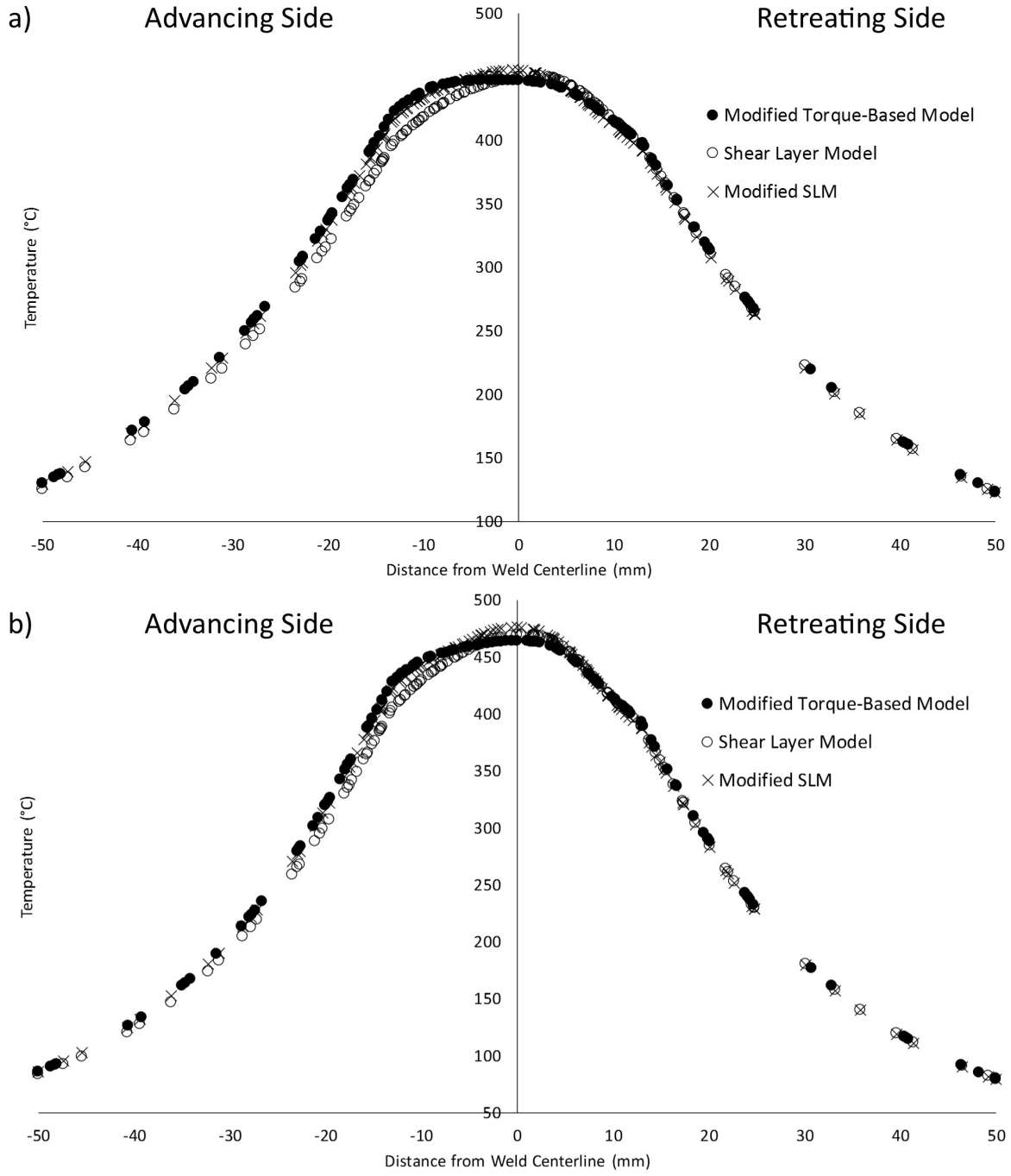

Fig. 4. Mid-plane temperature profiles with modified-SLM simulation added: a) 280/280 condition and b) 450/450 condition

taken at the mid-plane thickness just behind the pin as also done in the previous simulations. As seen in the figure, the modified-SLM shows strong agreement with both the torque-based and SLM temperature profiles.

Like the SLM simulation, the modified-SLM approach does not require welding forces, a coefficient of friction or a slip factor as inputs to the model, and as such, it adopts the flexibility of the SLM methodology. At the same time, the modified-SLM approach uses all tool/workpiece interfaces as heat generating surfaces like the torque-based approach. By utilizing an efficiency factor for frictional heat transfer, η_f, the modified-SLM approach strikes a balance between the convenience of the SLM approach and the realism of the modified torque-based approach.

4. Conclusions

A modified torque-based simulation was created to model the temperature distribution in aluminum 6082-T6 panels joined by friction stir welding. The simulation relied upon a slip factor and assumed coefficient of friction to model the heat flux at the tool/workpiece interfaces. The torque-based model was compared and contrasted against a shear layer approach (SLM) which circumvents the need for a slip factor and coefficient of friction, thus augmenting the convenience and flexibility of the model. Despite the difference between the two approaches, the temperature predictions were extremely similar. Analysis of the two models demonstrated that each approach ultimately predicted the same amount of total heat generation from the tool. The SLM approach, however, only modeled heat generation from the leading edges of the tool, while the torque-based approach modeled heat generation from all interfaces. In response to this discrepancy, a modified-SLM approach was proposed that modeled heat generation at all interfaces by utilizing a frictional heat transfer efficiency factor, η_f. By assigning a value of 0.5 to η_f, the modified-SLM approach showed excellent agreement with experimental temperatures and with the other two simulation approaches.

Acknowledgment

The authors acknowledge the AGH University of Science and Technology for the support of this research within the project no. 11.11.110.295.

REFERENCES

[1] R.S. Mishra, M.W. Mahoney, Friction Stir Welding and Processing, ASM International, Materials Park, OH, USA (2007).
[2] R.S. Mishra, P.S. De, N. Kumar, Friction Stir Welding and Processing, Springer International Publishing, New York, USA (2014).
[3] D. Lowasser, Z. Chen, Friction Stir Welding: From Basics to Applications, Woodhouse Publishing Limited, Cambridge, United Kingdom (2010).
[4] D.M. Neto, P. Neto, Int. J. Adv. Manuf. Technol. **65**, 115 (2013).
[5] K.J. Colligan, R.S. Mishra, Scr. Mater. **58**, 327 (2008).
[6] P. Kalya, K. Krishnamurthy, R.S. Mishra, J.A. Baumann, Friction Stir Welding and Processing IV (eds. R.S. Mishra, M.W. Mahoney, T.J. Lienert, K.V. Jata.), TMS, Orlando, FL, USA (2007).
[7] C. Hamilton, M.St. Węglowski, S. Dymek, Metall. Mater. Trans. B – Proc. Metall. Mater. Proc. Sci. **46**, 1409 (2015).
[8] W. Xie, E.C. De Meter, M.W. Trethewey, Int. J. Mach. Tools Manuf. **40,** 467 (2000).
[9] A. Mandal, B.S. Murty, M. Chakraborty, Wear **266**, 865 (2009).
[10] H. Schmid , J. Hattel, Scr. Mater. **58**, 332 (2008).
[11] K. J. Colligan, US Patent 6,669,075 (2003).
[12] P.L. Threadgill, M.M. Z. Ahmed, J.P. Martin, J.G. Perrett, B.P. Wynne, Thermec, Berlin, Germany (2009).
[13] J. Hilgert, H.N.B. Schmidt, J.F. Dos Santos, N. Huber, J. Mater. Process. Technol. **211**, 197 (2011).
[14] M.St. Węglowski, S. Dymek, Arch. Metall. Mater. **57**, 71 (2012).
[15] C. Hamilton, M. Kopyściański, O. Senkov, S. Dymek, Metall. Mater. Trans. A – Phys. Metall. Mater. Sci. **44**, 1730 (2013).
[16] Z. Gao, P. Wang, D. Cheng, J. Niu, C. Sommitsch, Engineering Review **35**, 283 (2015).
[17] A.M. Zahra, C.Y. Zahra, G. Jaroma-Weiland, G. Neuer, W. Lacom, J. Mater. Sci. **30**, 426 (1995).
[18] H. Wang, P. Colegrove, H.M. Mayer, L. Campbell, R.D. Robson, Advanced Materials Research **89-91**, 615 (2010).
[19] C. Hamilton, M. Kopyściański, A. Węglowska, S. Dymek, A. Pietras, Metall. Mater. Trans. A – Phys. Metall. Mater. Sci. **47**, 4519 (2016).
[20] C.C. Tutum, J.H. Hatel, Sci. Technol. Weld. Join. **15**, 369 (2010).
[21] American Society for Metals, Metals Handbook, 9th edition, The American Society for Metals (1979).
[22] R. Nandan, G.G. Roy, T.J. Leinert, T. Debroy, Acta Mater. **55**, 883 (2007).
[23] P. Heurtier, M.J. Jones, C. Desrayaud, J.H. Driver, F.Montheillet, D. Allehaux, J. Mater. Process. Technol. **171**, 348 (2006).